Geophysical Research Letters

RESEARCH LETTER
10.1029/2020GL089763

Key Points:

- Fast pathways connecting surface air to the North American UTLS occur over the eastern Pacific and the Gulf of Mexico
- A small fraction (10%) of tracers reaches the North American UTLS with ensemble-mean modal age <20 days
- Fast transport is associated with interaction between deep convection and resolved dynamics

Supporting Information:

- Supporting Information S1

Correspondence to:
X. Wang,
wang2807@purdue.edu

Citation:
Wang, X., Randel, W., & Wu, Y. (2021). Infrequent, rapid transport pathways to the summer North American upper troposphere and lower stratosphere. *Geophysical Research Letters*, *48*, e2020GL089763. https://doi.org/10.1029/2020GL089763

Received 7 JUL 2020
Accepted 23 NOV 2020

© 2020. American Geophysical Union. All Rights Reserved.

Infrequent, Rapid Transport Pathways to the Summer North American Upper Troposphere and Lower Stratosphere

Xinyue Wang[1,2], William Randel[2], and Yutian Wu[3]

[1]Department of Earth, Atmospheric and Planetary Sciences, Purdue University, West Lafayette, IN, USA, [2]Atmospheric Chemistry, Observations and Modeling Laboratory, National Center for Atmospheric Research, Boulder, CO, USA, [3]Lamont-Doherty Earth Observatory of Columbia University, Palisades, NY, USA

Abstract Transport pathways from the Northern Hemisphere surface into the North American upper troposphere-lower stratosphere (NA UTLS) during summertime are diagnosed from Boundary Impulse Response idealized tracers implemented at the Northern Hemisphere surface. In ensemble average, air masses enter the NA UTLS region via deep convection above Central America, and then slowly mix into the higher latitudes. However, fast transport pathways with a modal age around two weeks are evident in some tracer ensembles. For these rapid transport pathways, the tracers first reach the UTLS region over the eastern Pacific and the Gulf of Mexico as a result of enhanced deep convection and vertical advection, followed by horizontal transport over the United States by a stronger than normal UTLS anticyclone circulation.

Plain Language Summary Efficient pathways connecting surface air to the North American upper troposphere and lower stratosphere (NA UTLS) are important as short-lived tropospheric chemical species could survive transit into the lower stratosphere and hence affect ozone depletion. Our modeling study shows that the fast transport into the NA UTLS region can occur in a small fraction of cases with modal age <20 days. For these fast cases, the origin is enhanced deep convection over the eastern Pacific and the Gulf of Mexico, rather than locally over the contiguous United States. Deep convection controls transport from the boundary layer to 200 hPa, and then enhanced large-scale circulation, as a balanced response to the enhanced convection, dominates transport upwards into the UTLS region and toward southern United States following the NA monsoon anticyclonic flow.

1. Introduction

Observations and modeling studies have shown that the summer monsoon circulations are effective gateways of tropospheric air into the stratosphere (e.g., Randel et al., 2010; Vogel et al., 2019; Wu et al., 2020). Transport via the Asian and North American (NA) monsoons influences the composition of the upper troposphere and lower stratosphere (UTLS), which directly impacts the stratospheric chemistry and global radiative forcing (Anderson et al., 2017; Luo et al., 2018; Ordóñez et al., 2012; Solomon et al., 2011; Wales et al., 2018; Yu et al., 2015). Despite consensus on the pronounced UTLS chemical signals in both Asian and NA monsoon regions, the characteristics of monsoon-related troposphere-to-stratosphere transport and the underlying dynamics remain topics of active research.

The Asian summer monsoon (ASM)-related transport mainly consists of rapid uplifting from the surface to the convective outflow level by deep convections and typhoons, coupled with subsequent ascent and horizontal confinement by the large-scale ASM anticyclone in the UTLS (Gettelman and Forster, 2002; Pan et al., 2016; Park et al., 2007, 2008, 2009; Vogel et al., 2014). Recently, Wu et al. (2020) examined transport pathways linking the surface to the UTLS at 100 hPa using an idealized pulse passive tracer approach to reveal the transport dynamics. Fast transport paths were identified over the southern slope of the Tibetan Plateau, northern India, and Saudi Arabia with a modal age (the most probable transit time; see details in Section 2) of 5–10 days in an average of a large tracer ensemble. They demonstrated that the model-resolved vertical ascent controls the transport at 100–150 hPa while convective processes dominate around 200–300 hPa.

The NA UTLS exhibits similarities as well as differences with its Asian counterpart during summer. For instance, comparable stratospheric water vapor maxima are observed over both monsoon regions; however, the isotopic composition differs with enriched δD above North America but not over Asia, indicating different underlying thermodynamic processes (Randel et al., 2012). Aerosol layers are observed within both monsoon anticyclones around 100 hPa, but the vertical extent of the aerosol plume as well as its amplitude is much less over North America (Thomason & Vernier, 2013; Yu et al., 2015). Because of the very different topography, convection and large-scale circulations in the two regions, it is likely that the transport characteristics related to the North American summer monsoon (NASM) behave differently than those in Asia. While much progress has been made in understanding transport via the ASM during the past decades, studies on transport into the NA UTLS remain comparatively limited. There are several proposed mechanisms that may be responsible for the NA UTLS transport. Throughout the year, air gradually ascends into the stratosphere from the tropical upper troposphere, and then moves toward higher latitudes due to model-resolved horizontal transport (Abalos et al., 2013; Fueglistaler et al., 2004, 2009; Highwood & Hoskins, 1998; Vaughan & Timmis, 1998). In July and August, the NA UTLS is dominated by the anticyclone near 30°N, 110°W, owing to a Matsuno-Gill type response to the diabatic heating in the tropics and subtropics (Gill, 1980; Siu & Bowman, 2019). This large-scale anticyclone plays an important role in confinement of chemical species in the NA UTLS (Froyd et al., 2009; Randel et al., 2015; Solomon et al., 2011; Thomason & Vernier, 2013; Weinstock et al., 2007; Yu et al., 2015) and in increasing the residence time of air over the United States (Koby, 2016). In addition to the NASM convection, i.e., primarily located south of 30°N, overshooting storms become active in the contiguous United States, primarily over the north-central Great Plains, which could bring water vapor and surface pollutants to the UTLS (Cooney et al., 2018; Dessler & Sherwood, 2004; Jensen et al., 2020; Smith et al., 2017; Solomon et al., 2016). However, studies also found that a substantial fraction of moist air parcels at 100 hPa in the 20°N–40°N latitudinal range cannot be explained by nearby deep convection (Sun & Huang, 2015). Therefore, an investigation of the relative contributions due to distinct pathways and their transport timescales into the NA UTLS is needed to interpret observations and to assess and improve the model performance in simulating processes in the UTLS.

In this study, we focus on the most efficient route connecting the Northern Hemisphere (NH) surface and the NA UTLS due to its implication for transporting very short-lived (VSL) trace gas pollutants which can deplete stratospheric ozone (Hossaini et al., 2015; Levine et al., 2007). Specifically, we aim to address three questions: (1) Are there relatively efficient transport pathways from the boundary layer into the NA UTLS during summer? (2) What is the timescale for the fast transport? (3) What is the dynamical mechanism? To isolate the role of dynamics from other factors such as lower tropospheric chemistry and surface emissions, we apply the idealized pulse passive tracer approach (to be discussed later) and use the same model experiment as in Wu et al. (2020). The numerical model experiment and diagnostics will be described in the following section.

2. Methods

We apply the "Boundary Impulse Response (BIR)," or known as the pulse tracer approach to diagnose transport characteristics linking the NH surface to the NA UTLS. This approach has been commonly used to study the atmospheric transport (Orbe et al., 2012, 2013, 2016). Specifically, the BIR of a location contains information on the distribution of times since a pulse of passive tracer last contacted the NH surface. The Green's function or distribution of transit times captures all possible pathways connecting the source region and the receptor surface, and allows us to identify the most efficient route. The modal age is defined as the mode of Green's function, or the peak time of the tracer evolution. The diagnostics are performed with the Whole Atmosphere Community Climate Model version 5 (WACCM5) in atmosphere-only mode. The model resolution is 0.95° latitude × 1.25° longitude (~100 km) with 110 pressure layers (~0.5 km spacing above the boundary layer and in the lower stratosphere). Hereafter, we refer to this model as WACCM5-L110. Deep convection is treated by Zhang and McFarlane (1995) with improved convective momentum transport (Richter & Rasch, 2008; Tilmes et al., 2016) and shallow convection is treated as described by Park and Bretherton (2009). WACCM5-L110 includes a number of improvements to standard WACCM configuration with 70 vertical levels. Wang et al. (2018) reported that simulations by this model agree well with reanalysis data and observations with regard to the wind and temperature climatologies as well as stratospheric water vapor distribution. Further information on WACCM5-L110 is summarized in Garcia and Richter (2019).

Our tracer implementation is identical to that presented in Wu et al. (2020). Specifically, the pulse tracer is released at the boundary layer over the entire NH with concentration being set to 1 mol/mol only during the first day. The passive tracer has no specific sources/sinks or chemical reactions in the atmosphere interior. Its concentration is set to zero whenever the tracer is in contact with the surface again after its release. The transport of tracer is driven by both resolved and parameterized processes in the model. For each summer (July and August), we implement 10 tracers and release them on different days, i.e., on 3, 10, 17, 24, and 31 July and 3, 10, 17, 24, and 31 August, respectively, to explicitly assess how the transport properties vary with synoptic variability of the monsoonal system. We examine statistics from 90 tracers, i.e., nine-year simulations including 1981–1987, 1989, and 1990. The model is integrated from January 1981 to December 1994 with prescribed sea surface temperatures and sea ice.

What processes account for the fast transport from the NH surface to the NA UTLS? To evaluate this, we turn to the tracer budget as follows:

$$\frac{\partial T_x}{\partial t} = TAT_x + VDT_x + TCOND_T_x + TCONS_T_x, \tag{1}$$

with T_x the tracer concentration, corresponding to the mass fraction of air that had last contact with NH surface at any time in the past, TAT_x, VDT_x, $TCOND_T_x$, and $TCONS_T_x$ the transport tendency due to the resolved dynamics, vertical diffusion, deep convection, and shallow convection, respectively, which are calculated by the model and saved at daily time step. Tracer budget analysis allows us to separate different transport processes and assess the influence of each component explicitly. The resolved dynamics term can be further decomposed into horizontal and vertical advection components as follows:

$$TAT_x = \underbrace{-\frac{u}{acos\phi}\frac{\partial T_x}{\partial \lambda}}_{\text{horizontal advection}} \underbrace{-\frac{v}{a}\frac{\partial T_x}{\partial \phi} \quad -\omega\frac{\partial T_x}{\partial p}}_{\text{vertical advection}}, \tag{2}$$

where u, v, and ω denote the zonal velocity, meridional velocity, and vertical velocity in pressure coordinates, respectively. p denotes the pressure value. a is the radius of the Earth. ϕ and λ are the latitude and longitude, respectively.

3. Results

To characterize the transport timescales from the surface into the NA UTLS, we analyze the daily evolution of the 90 tracers averaged over the box defined by 10°N–40°N and 140°W–60°W at 110 hPa (see Figure 1a). The tropopause height is typically located above 150 hPa over the NASM region during July and August months (see Figure S1), thus pressure level of 110 hPa is in the lower stratosphere. The boxed region is the same as that in Randel et al. (2015), where maxima in UTLS water vapor are observed. The modal ages in Figure 1a, corresponding to the peak values of each BIR Green's function averaged over the boxed area, exhibit a widespread distribution (see also Figure S2), resulting from a variety of transport pathways. Transit along some paths takes >2 months (66 days), while along others it occurs within 3 days. Sorting the modal times of each BIR over the boxed area allows us to categorize the "normal" ensemble where the modal age falls between the 10th and 90th percentile (23–55 days). The black curve is the average of the normal ensembles, peaking on day 40 and decaying slowly. Accordingly, Figure 1b shows the composited modal age distribution for these normal ensembles at 110 hPa. The fastest modal times in Figure 1b occur above Central America, equatorial Pacific, and Atlantic Ocean, on a modal timescale of 14–21 days. The transport timescale gradually increases toward higher latitudes due to the quasi-horizontal eddy transport by the North American anticyclone (Abalos et al., 2013). In general, transport to the UTLS in the vicinity of the NASM is slower than that of the ASM, largely related to the weaker monsoon strength and lower altitude range of the anticyclone compared to its Asian counterpart (Nützel et al., 2019; Yan et al., 2019). Blue lines in Figure 1a highlight the fast ensemble members whose model age falls below the 10th percentile, with an ensemble mean modal age of 17 days. Figure 1c shows the composited modal age distribution for the fast ensembles at 110 hPa. The fastest transport pathway shifts northward to 20°N and occurs above the eastern Pacific and the Gulf of Mexico, with a regional modal age of 14 days. Analysis at 100 hPa yields similar

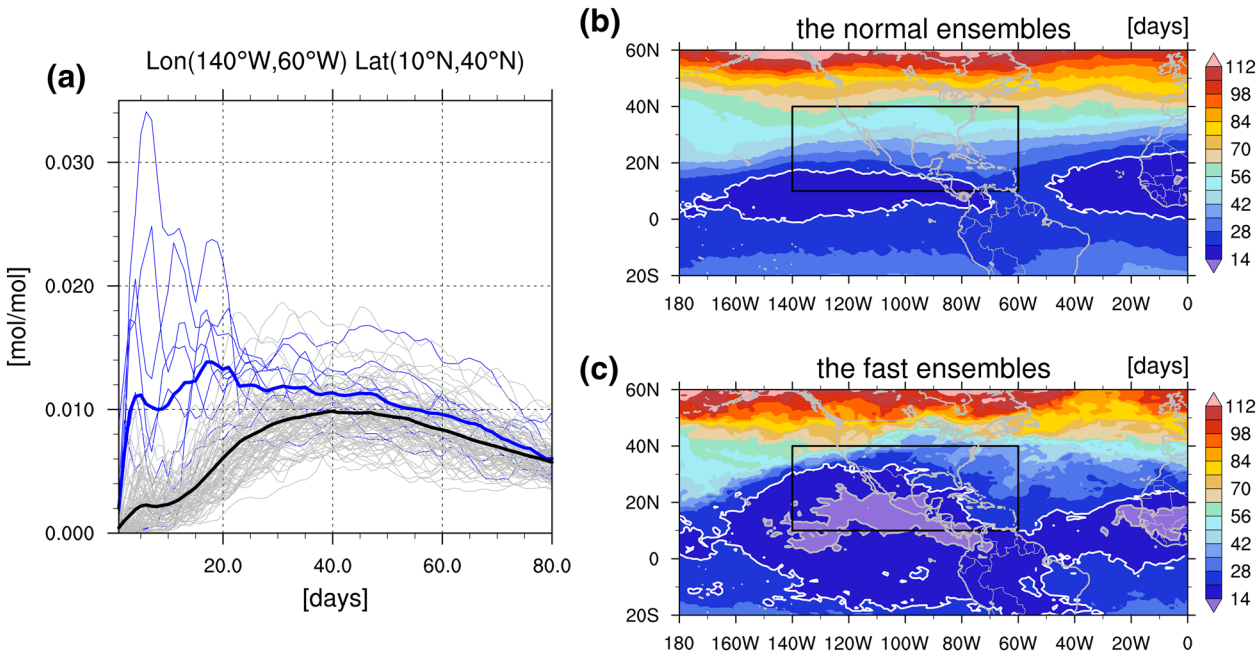

Figure 1. (a) Gray lines plot tracer mixing ratio evolution averaged over 10°N–40°N and 140°W–60°W (black-boxed region on the right) at 110 hPa as a function of elapsed time. Blue lines indicate the fast transport ensembles with modal ages below the 10th percentile, and the thick blue line is their mean. The thick black line is the mean of normal tracer ensemble whose modal age falls between the 10th and 90th percentile. (b) The averaged modal ages of normal ensemble. Similarly, (c) the averaged modal ages of fast tracer ensemble represented by blue lines in (a). Gray and white contours highlight 14 and 21 days of modal age, respectively.

conclusions on the transport paths and timescales (not shown). However, the composited features of the fast ensembles at 100 hPa are dominated by three extreme cases. Though results are statistically significant at the 95% confidence level using bootstrap method, we are concerned about the small sample size. Therefore, we choose to present results at 110 hPa pressure level.

We now examine the day-to-day evolution of the fast ensembles compared to the normal ensembles by evaluating the average BIR during different periods, i.e., over 1–2, 3–5, 6–8, and 9–14 days after the first day of tracer release. Figure 2 displays the ensemble mean tracer concentration differences between the fast and normal cases at 110 hPa, at 25°N, and in zonal mean between 140°W and 60°W. During days 1–2, very rapid and strong uplift of tracers into the NA UTLS region occurs preferentially over the Gulf of Mexico and the eastern Pacific. During days 3–5, a substantial increase is seen above northwest Mexico. In addition to vertical transport by deep plumes near 90°W, 20°N, horizontal advection can be seen in both zonal and meridional directions. Tracers are transported westward and equatorward, especially in the upper troposphere. During days 6–8, tracers are advected northeastward and maximize above the subtropical eastern Pacific and the Gulf of California. During days 9–14, tracers are separated from the tropics, and are confined above the southern United States. However, for normal ensembles, there is nearly indistinguishable tracer enhancement above the North American Southwest. The vast majority of tracers arrives at the UTLS in the Western Hemisphere near 10°N, especially above northern Africa.

Tracer budget analyses are used to examine the contributions from individual processes following Equation 1 averaged over the boxed region 10°N–40°N and 140°W–60°W. To obtain a general picture, we calculate and plot the vertical profiles of the relative contribution of each term using the average of 90 BIR tracers during the first week (see Figure S3). In fact, calculations composited for the fast and normal ensembles yield profiles with comparable amplitude peaks throughout the atmosphere (not shown). The transport tendency in the mid-to-upper troposphere, especially from 400 to 300 hPa, is largely attributed to the nearby deep convection, and partly by the resolved dynamics. The shallow convection-driven and vertical diffusion-driven transport processes are relatively weaker. Above 300 hPa, the contribution due to deep convection decreases rapidly with altitudes where the resolved dynamics-driven transport takes over, together with

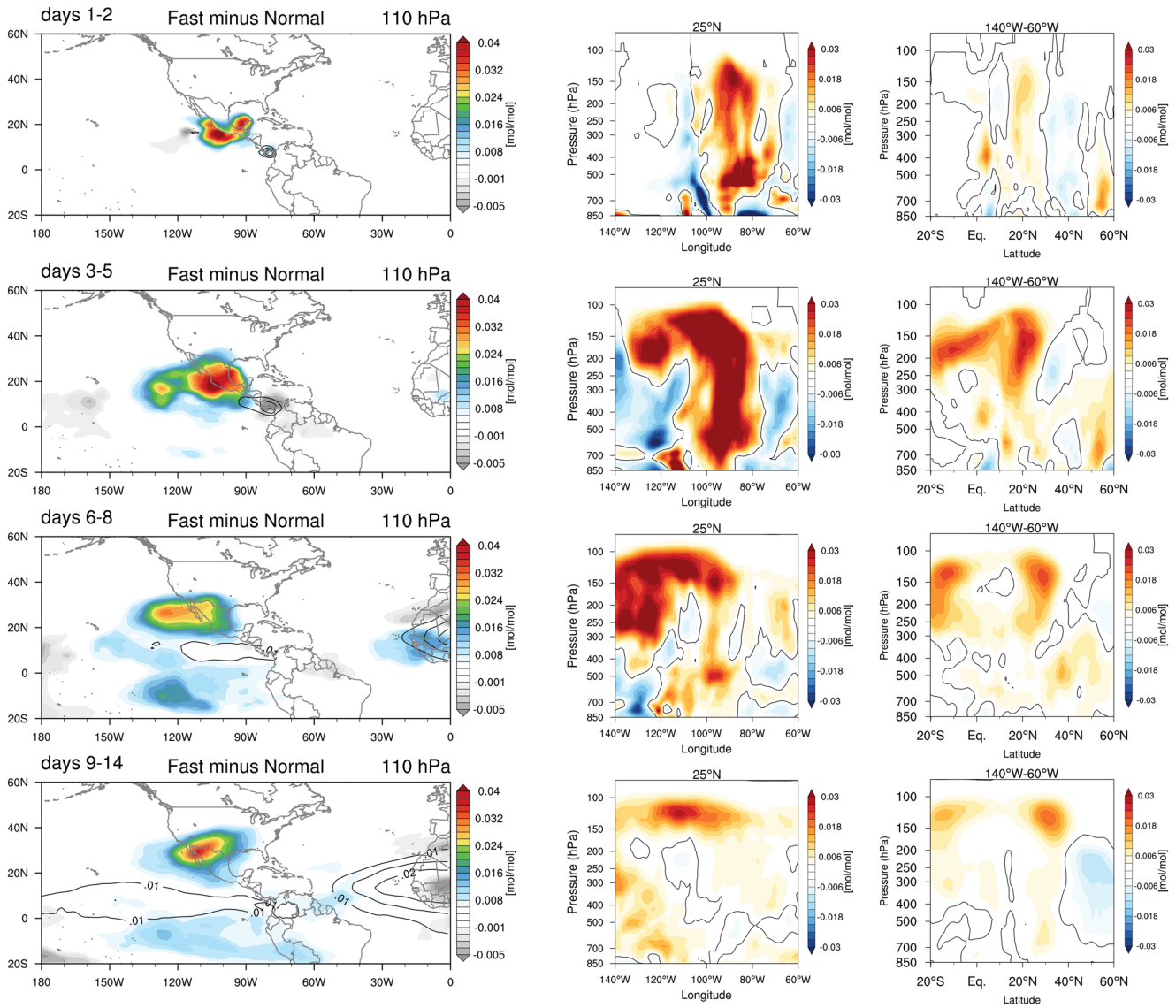

Figure 2. Color shadings are tracer evolution differences between the fast and the normal ensemble at 110 hPa (left column), the vertical-longitudinal cross sections at 25°N (middle column), and the vertical-latitudinal cross-sections averaged between 140°W and 60°W (right column) during days 1–2 (first row), days 3–5 (second row), days 6–8 (third row), and days 9–14 (fourth row). The units are mol/mol. Black contours in the left column denote the averaged tracer concentrations of the normal ensembles while denote the zero contour lines in the middle and right columns.

a small contribution from vertical diffusion. The Costa Rica Aura Validation Experiment campaign has observed a sharp drop in aerosol composition at 200 hPa, which is linked to the abrupt decrease of convective influence (Froyd et al., 2009). Coherent behaviors are also seen in another artificial tracer study based on e90 [Figure 11c in Abalos et al. (2017)]. Overall, both deep convection and resolved dynamics play principal roles in transport into the NA UTLS region, consistent with the processes of its Asian counterpart (Wu et al., 2020). More precisely, while deep convection determines the gradient of tracer concentrations at the bottom of the UTLS with transport times of several hours to 1–2 days in WACCM5, the resolved large-scale circulation governs the transport further upward with typical transport times of several weeks.

The leading mechanisms responsible for the fast transport into the NA UTLS are evaluated by contrasting to conditions of the normal ensembles. Because the difference in area-averaged convective transport ($TCOND_T_x$) is most pronounced at 200 hPa during the first 2 days (not shown), we first show the horizontal distribution of the composited 200 hPa $TCOND_T_x$ for the fast ensembles, normal ensembles, and their

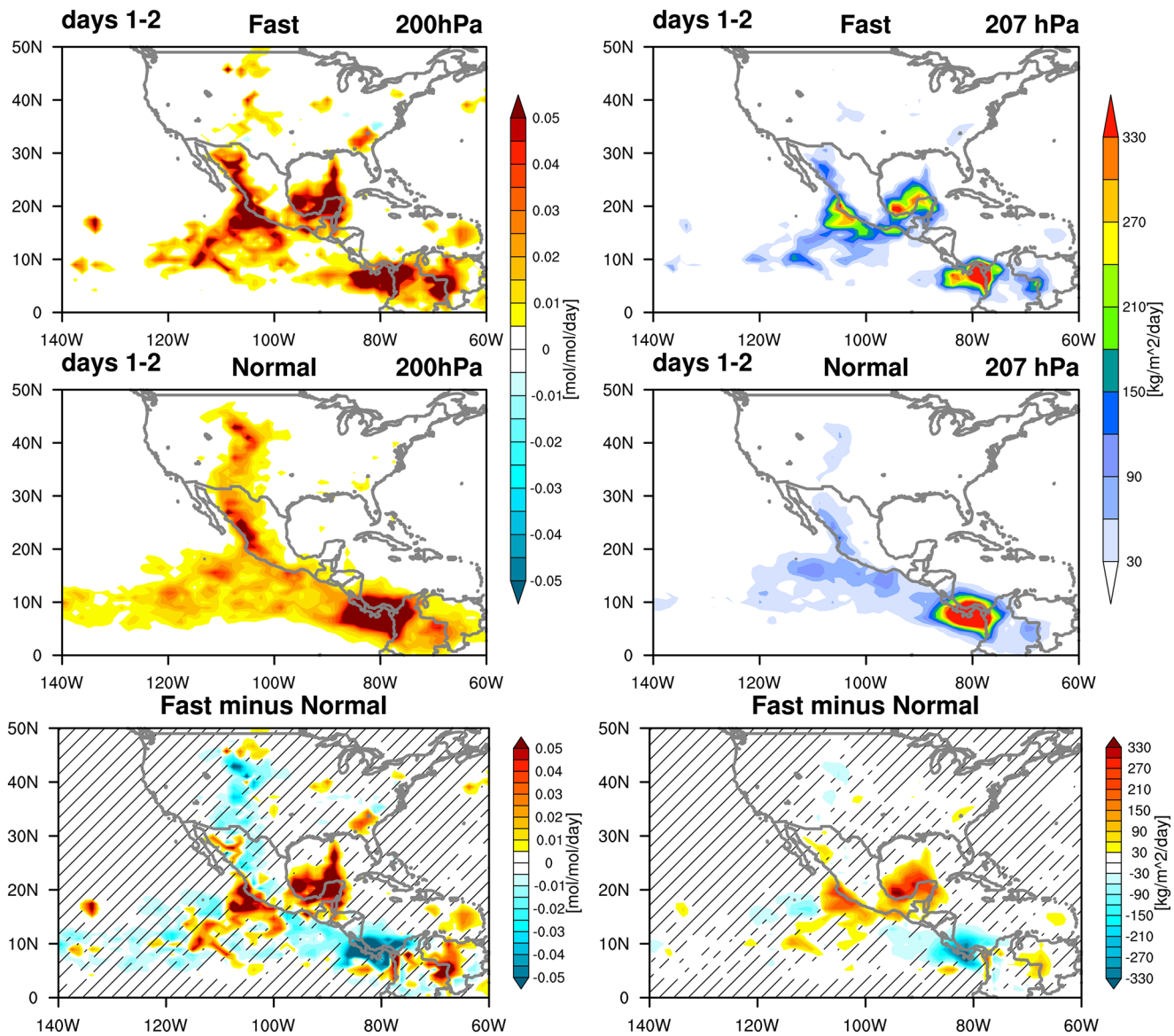

Figure 3. Left panels show deep convection-driven transport tendency at 200 hPa for the fast ensembles (top row), the normal ensembles (middle row), and their difference (bottom row) in days 1–2. Right panels show the composited convective mass flux from Zhang-McFarlane (ZM) scheme (kg/m^2/day) at 207 hPa for the fast ensembles (top row), the normal ensembles (middle row), and their difference (bottom row) in days 1–2. The hatching denotes the region where the differences are not statistically significant at the 95% confidence level using the bootstrap method.

differences, respectively, in the left column of Figure 3. For normal ensembles, the deep convection-driven transport tendency shows a localized maximum between 0°N and 10°N, consistent with the observed heaviest precipitation in tropical Central America and the northern part of South America (Randel et al., 2015; Siu & Bowman, 2019). In contrast to the climatological maxima of tracer transport in the tropics, stronger positive tendency due to deep convection is found north of 15°N in the fast ensembles, clustering around the Gulf of Mexico, northwestern Mexico (i.e., Sierra Madre Occidental), and southern Mexico (i.e., southwest slope of Sierra Madre del Sur). Meanwhile, there is anomalously weak transport tendency along the Great Plains in the fast ensembles compared to the normal. The convection driven transport tendency at 200 hPa becomes weak and statistically insignificant from the third day onward (not shown). In addition, we also examine the convective mass flux from Zhang-McFarlane (ZM) scheme, which is the direct measure of convective transport, to confirm our findings. Coherent patterns of convective mass flux around 200 hPa are evident on the right column of Figure 3, i.e., the large positive transport tendency is collocated with

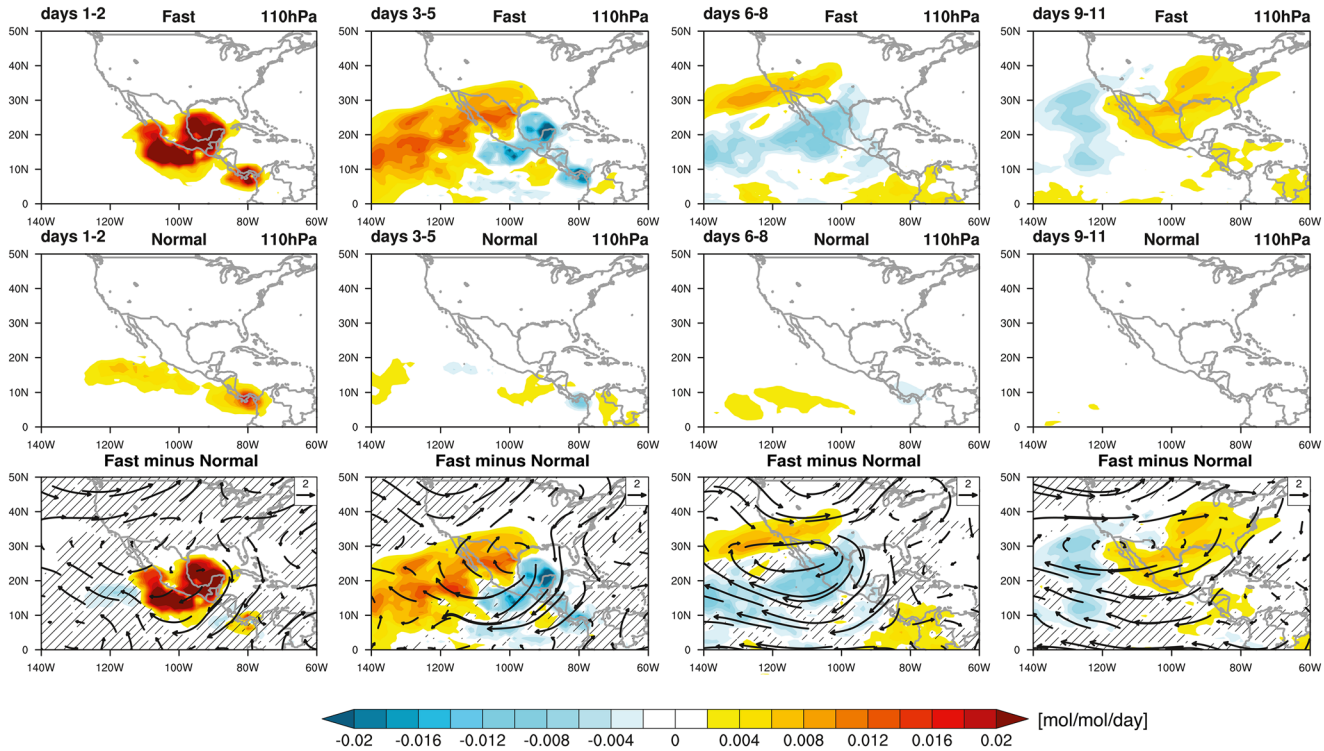

Figure 4. Resolved dynamics-driven transport tendency at 110 hPa for the fast ensembles (first row), the normal ensembles (second row), and their differences (third row) in days 1–2 (first column), days 3–5 (second column), days 6–8 (third column), and days 9–11 (fourth column). The vectors in the third row are horizontal wind differences between the fast and the normal ensembles. The hatching is the same as in Figure 3.

stronger convection over the Gulf of Mexico and the eastern Pacific. Vertical cross section of the composited convective mass flux averaged between 140°W and 60°W (Figure S4) shows intensified convection ranging from 20°N to 30°N whereas weaker convection over the US continent from 30°N to 45°N during the fast transport.

Evolution of the resolved dynamics-driven transport at 110 hPa is highlighted in Figure 4, comparing the fast and normal ensembles. For days 1–2, strong transport tendency occurs above the Gulf of Mexico and the west coast of Mexico, collocated with increased tracer concentration at 110 hPa in Figure 2. During days 3–5 westward movement of the tracers increases tendencies over the subtropical Pacific Ocean, linked to anomalously strong UTLS anticyclonic circulation. This behavior continues over days 6–8, contributing to tracer increases along the eastern Pacific at 30°N and reaching the southwestern US continent, which is in agreement with the northward shift of the tracer concentration (Figure 2). Over days 9–11, widespread positive tendency occurs above the southeastern US continent and Mexico. In comparison, the tracer tendency due to resolved circulation for the normal ensembles is much weaker in the subtropics during the first 2 weeks (Figure 4, middle row). The bottom panel of Figure 4 shows the TAT_x difference between the top and middle panels and the superimposed vectors are the associated horizontal wind difference. The differences highlight a persistent anomalous anticyclonic circulation over the southern US continent during the first 2 weeks, consistent with the horizontal tracer transport over the US. This is an important component of the systematic fast transport pathways ending over the continental US. We further decompose the resolved dynamics term related to the fast transport into vertical and horizontal components following Equation 2 (see Figure S5). During the first 2 weeks, persistent positive transport tendency due to the vertical advection appears above the Gulf of Mexico and the eastern Pacific, constantly uplifting the tracers to 110 hPa via these regions. But this is largely compensated by negative contribution due to the horizontal advection, which transports the tracers toward the continental US via the intensified upper-level anticyclone.

To summarize the mechanism resulting in the fast transport, Figure 5 shows the vertical structure of composite differences between the fast and normal ensembles for temperature, meridional wind, and vertical

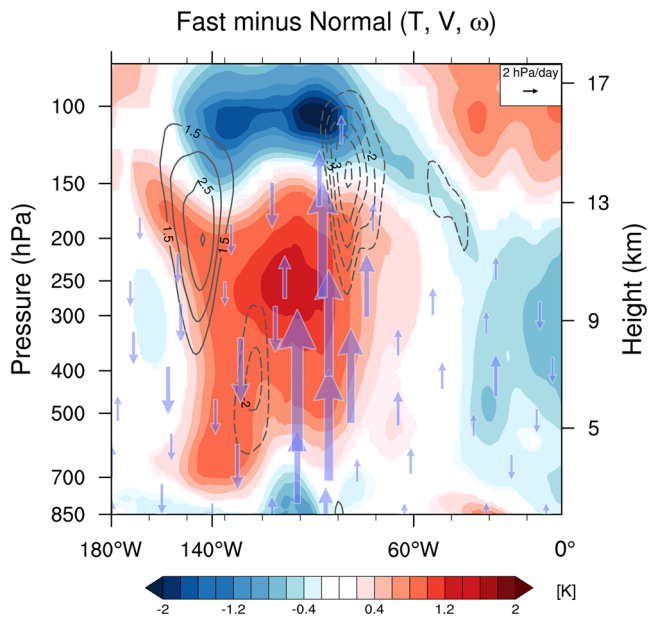

Figure 5. The composited differences between the fast and the normal ensemble for temperature (K, shaded), meridional winds (in contour with 1 m/s interval), and vertical velocities ω (hPa/day, in arrow). Variables are averaged between 10°N and 40°N during days 1–14. Regions where temperature differences are not significant at the 95% level using the bootstrap method are shaded white.

motion averaged over the latitudinal band of 10°N to 40°N. The latent heat released by the stronger than normal convection in 20°N–30°N latitudes (i.e., the Gulf of Mexico and the eastern Pacific; Figure 3) leads to an intensified upward transport extending into the UTLS region and a warm anomaly in the tropospheric column. In response to the stronger convective forcing, the upper-level anticyclonic circulation is strengthened above the southern US. The strong ascent (descent) is coupled with increased northerly (southerly) in the UTLS via Sverdrup balance; i.e., $\beta v \approx f\,(\partial\omega/\partial p)$, where f is the Coriolis parameter and β is its meridional gradient (Garny & Randel, 2013; Gill, 1980; Siu & Bowman, 2019; Wu & Shaw, 2016). The net effect is that tracers are efficiently advected upward and then are confined and circulated by the intensified anticyclone caused by stronger and northward displaced convection.

4. Conclusion

In this study, we employ the pulse passive tracer approach implemented in WACCM5-L110 to study transport processes connecting the NH boundary layer to the NA UTLS during summer months. Understanding transport paths and associated transit times are important in interpreting and modeling the behavior of chemical species in the UTLS. We focus on the fast pathway due to its potential for uplifting VSL ozone depleting substances into the lower stratosphere (e.g., Luo et al., 2018; Ordóñez et al., 2012; Wales et al., 2018). In addition, we explicitly evaluate the budget of the pulse tracers to investigate the leading mechanism for the fast transport.

Previous studies have documented two important transport pathways to the NA UTLS (Abalos et al., 2013; Fueglistaler et al., 2009; Jensen et al., 2020; Smith et al., 2017). The primary but slow path occurs via the tropical upper troposphere associated with the large-scale Brewer-Dobson circulation, followed by ascent into the stratosphere and progressing poleward toward higher latitudes. Our study shows that the climatological strongest convection and vertical transport occurs over central America, and once the tracer is lifted to the upper troposphere it is advected westward to the eastern tropical Pacific. The transport to the US is via a relatively slow diffusive process with a modal age of 40 days. Another proposed direct and rapid transport pathway involves overshooting convection over the north-central Great Plains. Despite possible biases in the representation of convection in WACCM5, we evaluate its simulation of tropopause overshooting convection (see Figure S6) against observations. We find a similar spatial distribution of overshoots to observations with a frequency of one event within most grid boxes per decade north of 35°N during July and August (Cooney et al., 2018), despite the differences in the time period and horizontal resolution between the model simulation and observations. However, the overshooting convection does not contribute substantially to the UTLS tracer budget compared to the resolved circulation in these results. In this study, we find that the fast path to the NA UTLS occurs via strong convection and large-scale ascent over the Gulf of Mexico and the eastern Pacific at 15°N–20°N and horizontal advection by the upper-level anticyclone to the US, rather than locally over the contiguous United States. The pathway occurs on a mean modal age of about 17 days, possibly allowing transport of VSL halocarbons of oceanic origin into the NA UTLS. Although the overall transport in the vicinity of the NA monsoon is slow compared to its Asian counterpart whose modal age is about 5–20 days during July and August, largely due to its weaker convection and large-scale ascent, we find that the resolved dynamics plays a critical role in tracer transport in the UTLS over both monsoon regions (Wu et al., 2020). However, we note that these conclusions could possibly depend on the model resolution and the treatment of convection within WACCM5-L110.

Overall, our results demonstrate the importance of interaction between deep convection and resolved dynamics in rapid uplifting of the tracer into the NA UTLS region and have important implications for understanding the chemical constituents in NA UTLS. Future work will explore the sensitivity of these results to model's representation of convection.

Data Availability Statement

Model data are made available through http://kage.ldeo.columbia.edu:81/SOURCES/.LDEO/.Climate-Group/.PROJECTS/.PublicationsData/.Wu_etal_JGR_2019. X. Wang and Y. Wu are supported by the NSF Award AGS-1802248. Most of the work was carried out during visit of X. Wang to the ACOM lab, sponsored by the Advanced Study Program Graduate Visitor Program.

Acknowledgments
The authors appreciate the constructive discussion with the UTLS group at the Atmospheric Chemistry Observations and Modeling (ACOM) Division, NCAR. The authors also thank Drs Eric Jensen, Cameron Homeyer, Marta Abalos, Hao Ye, Clara Orbe, and Ben Li for helpful suggestions. The authors sincerely thank two anonymous reviewers for their valuable comments, which helped to greatly improve the manuscript. The model experiments were carried out with high-performance computing support provided by NCAR's Computational and Information Systems Laboratory, sponsored by the National Science Foundation (NSF).

References

Abalos, M., Randel, W., Kinnison, D., & Serrano, E. (2013). Quantifying tracer transport in the tropical lower stratosphere using WACCM. *Atmospheric Chemistry and Physics*, *13*(10), 10591–10607.

Abalos, M., Randel, W. J., Kinnison, D. E., & Garcia, R. R. (2017). Using the artificial tracer e90 to examine present and future UTLS tracer transport in WACCM. *Journal of the Atmospheric Sciences*, *74*(10), 3383–3403.

Anderson, J. G., Weisenstein, D. K., Bowman, K. P., Homeyer, C. R., Smith, J. B., & Wilmouth, D. M. (2017). Stratospheric ozone over the United States in summer linked to observations of convection and temperature via chlorine and bromine catalysis. *Proceedings of the National Academy of Sciences of the United States of America*, *114*(25), E4905–E4913.

Cooney, J. W., Bowman, K. P., Homeyer, C. R., & Fenske, T. M. (2018). Ten year analysis of tropopause-overshooting convection using GridRad data. *Journal of Geophysical Research: Atmospheres*, *123*(1), 329–343. https://doi.org/10.1002/2017JD027718

Dessler, A., & Sherwood, S. (2004). Effect of convection on the summertime extratropical lower stratosphere. *Journal of Geophysical Research: Atmospheres*, *109*, D23301. https://doi.org/10.1029/2004JD005209

Froyd, K. D., Murphy, D. M., Sanford, T. J., Thomson, D. S., Wilson, J. C., Pfister, L., & Lait, L. (2009). Aerosol composition of the tropical upper troposphere. *Atmospheric Chemistry and Physics*, *9*(13), 4363–4385. https://doi.org/10.5194/acp-9-4363-2009

Fueglistaler, S., Dessler, A., Dunkerton, T., Folkins, I., Fu, Q., & Mote, P. W. (2009). Tropical tropopause layer. *Reviews of Geophysics*, *47*(1), RG1004. https://doi.org/10.1029/2008RG000267

Fueglistaler, S., Wernli, H., & Peter, T. (2004). Tropical troposphere-to-stratosphere transport inferred from trajectory calculations. *Journal of Geophysical Research: Atmospheres*, *109*, D03108. https://doi.org/10.1029/2003JD004069

Garcia, R. R., & Richter, J. H. (2019). On the momentum budget of the quasi-biennial oscillation in the whole atmosphere community climate model. *Journal of the Atmospheric Sciences*, *76*(1), 69–87.

Garny, H., & Randel, W. (2013). Dynamic variability of the Asian monsoon anticyclone observed in potential vorticity and correlations with tracer distributions. *Journal of Geophysical Research: Atmospheres*, *118*(24), 13421–13433. https://doi.org/10.1002/2013JD020908

Gettelman, A., & Forster, P. (2002). A climatology of the tropical tropopause layer. *Journal of the Meteorological Society of Japan. Series II*, *80*(4B), 911–924.

Gill, A. E. (1980). Some simple solutions for heat-induced tropical circulation. *Quarterly Journal of the Royal Meteorological Society*, *106*(449), 447–462.

Highwood, E., & Hoskins, B. (1998). The tropical tropopause. *Quarterly Journal of the Royal Meteorological Society*, *124*(549), 1579–1604.

Hossaini, R., Chipperfield, M., Montzka, S., Rap, A., Dhomse, S., & Feng, W. (2015). Efficiency of short-lived halogens at influencing climate through depletion of stratospheric ozone. *Nature Geoscience*, *8*(3), 186–190.

Jensen, E., Pan, L. L., Honomichl, S., Diskin, G. S., Krämer, M., & Spelten, N. (2020). Assessment of observational evidence for direct convective hydration of the lower stratosphere. *Journal of Geophysical Research: Atmospheres*, *125*(15), e2020JD032793. https://doi.org/10.1029/2020JD032793

Koby, T. R. (2016). *Development of a trajectory model for the analysis of stratospheric water vapor (Unpublished doctoral dissertation)*. Cambridge, MA: Harvard University.

Levine, J., Braesicke, P., Harris, N., Savage, N., & Pyle, J. (2007). Pathways and timescales for troposphere-to-stratosphere transport via the tropical tropopause layer and their relevance for very short lived substances. *Journal of Geophysical Research: Atmospheres*, *112*, D04308. https://doi.org/10.1029/2005JD006940

Luo, Z. J., Pan, L. L., Atlas, E. L., Chelpon, S. M., Honomichl, S. B., Apel, E. C., & Hall, S. R. (2018). Use of airborne in situ VOC measurements to estimate transit time spectrum: An observation-based diagnostic of convective transport. *Geophysical Research Letters*, *45*(23), 13150–13157. https://doi.org/10.1029/2018GL080424

Nützel, M., Podglajen, A., Garny, H., & Ploeger, F. (2019). Quantification of water vapour transport from the Asian monsoon to the stratosphere. *Atmospheric Chemistry and Physics*, *19*(13), 8947–8966.

Orbe, C., Holzer, M., & Polvani, L. M. (2012). Flux distributions as robust diagnostics of stratosphere-troposphere exchange. *Journal of Geophysical Research: Atmospheres*, *117*, D01302. https://doi.org/10.1029/2011JD016455

Orbe, C., Holzer, M., Polvani, L. M., & Waugh, D. (2013). Air-mass origin as a diagnostic of tropospheric transport. *Journal of Geophysical Research: Atmospheres*, *118*(3), 1459–1470. https://doi.org/10.1002/jgrd.50133

Orbe, C., Waugh, D. W., Newman, P. A., & Steenrod, S. (2016). The transit-time distribution from the Northern Hemisphere midlatitude surface. *Journal of the Atmospheric Sciences*, *73*(10), 3785–3802.

Ordóñez, C., Lamarque, J.-F., Tilmes, S., Kinnison, D. E., Atlas, E. L., Blake, D. R., & Saiz-Lopez, A. (2012). Bromine and iodine chemistry in a global chemistry-climate model: Description and evaluation of very short-lived oceanic sources. *Atmospheric Chemistry and Physics*, *12*(3), 1423–1447.

Pan, L. L., Honomichl, S. B., Kinnison, D. E., Abalos, M., Randel, W. J., Bergman, J. W., & Bian, J. (2016). Transport of chemical tracers from the boundary layer to stratosphere associated with the dynamics of the Asian summer monsoon. *Journal of Geophysical Research: Atmospheres*, *121*(23), 14159–14174. https://doi.org/10.1002/2016JD025616

Park, M., Randel, W. J., Emmons, L. K., Bernath, P. F., Walker, K. A., & Boone, C. D. (2008). Chemical isolation in the Asian monsoon anticyclone observed in Atmospheric Chemistry Experiment (ACE-FTS) data. *Atmospheric Chemistry and Physics*, *8*(3), 757–764.

Park, M., Randel, W. J., Emmons, L. K., & Livesey, N. J. (2009). Transport pathways of carbon monoxide in the Asian summer monsoon diagnosed from Model of Ozone and Related Tracers (MOZART). *Journal of Geophysical Research: Atmospheres*, *114*, D08303. https://doi.org/10.1029/2008JD010621

Park, M., Randel, W. J., Gettelman, A., Massie, S. T., & Jiang, J. H. (2007). Transport above the Asian summer monsoon anticyclone inferred from Aura microwave limb sounder tracers. *Journal of Geophysical Research: Atmospheres*, *112*, D16309. https://doi.org/10.1029/2006JD008294

Park, S., & Bretherton, C. S. (2009). The University of Washington shallow convection and moist turbulence schemes and their impact on climate simulations with the Community Atmosphere Model. *Journal of Climate*, *22*(12), 3449–3469.

Randel, W. J., Moyer, E., Park, M., Jensen, E., Bernath, P., Walker, K., & Boone, C. (2012). Global variations of HDO and HDO/H2O ratios in the upper troposphere and lower stratosphere derived from ACE-FTS satellite measurements. *Journal of Geophysical Research: Atmospheres*, *117*, D06303. https://doi.org/10.1029/2011JD016632

Randel, W. J., Park, M., Emmons, L., Kinnison, D., Bernath, P., Walker, K. A., & Pumphrey, H. (2010). Asian monsoon transport of pollution to the stratosphere. *Science*, *328*(5978), 611–613.

Randel, W. J., Zhang, K., & Fu, R. (2015). What controls stratospheric water vapor in the NH summer monsoon regions? *Journal of Geophysical Research: Atmospheres*, *120*(15), 7988–8001. https://doi.org/10.1002/2015JD023622

Richter, J. H., & Rasch, P. J. (2008). Effects of convective momentum transport on the atmospheric circulation in the Community Atmosphere Model, version 3. *Journal of Climate*, *21*(7), 1487–1499.

Siu, L. W., & Bowman, K. P. (2019). Forcing of the upper-tropospheric monsoon anticyclones. *Journal of the Atmospheric Sciences*, *76*(7), 1937–1954.

Smith, J. B., Wilmouth, D. M., Bedka, K. M., Bowman, K. P., Homeyer, C. R., Dykema, J. A., & others (2017). A case study of convectively sourced water vapor observed in the overworld stratosphere over the United States. *Journal of Geophysical Research: Atmospheres*, *122*(17), 9529–9554. https://doi.org/10.1002/2017JD026831

Solomon, D. L., Bowman, K. P., & Homeyer, C. R. (2016). Tropopause-penetrating convection from three-dimensional gridded NEXRAD data. *Journal of Applied Meteorology and Climatology*, *55*(2), 465–478.

Solomon, S., Daniel, J. S., Neely, R. R., Vernier, J.-P., Dutton, E. G., & Thomason, L. W. (2011). The persistently variable "background" stratospheric aerosol layer and global climate change. *Science*, *333*(6044), 866–870.

Sun, Y., & Huang, Y. (2015). An examination of convective moistening of the lower stratosphere using satellite data. *Earth and Space Science*, *2*(7), 320–330. https://doi.org/10.1002/2015EA000115

Thomason, L., & Vernier, J.-P. (2013). Improved SAGE II cloud/aerosol categorization and observations of the Asian tropopause aerosol layer: 1989-2005. *Atmospheric Chemistry and Physics*, *13*(9), 4605.

Tilmes, S., Lamarque, J.-F., Emmons, L. K., Kinnison, D. E., Marsh, D., Garcia, R. R., ... others (2016). Representation of the community Earth system model (CESM1) CAM4-chem within the chemistry-climate model initiative (CCMI). *Geoscientific Model Development Discussions*, *9*, 1853–1890.

Vaughan, G., & Timmis, C. (1998). Transport of near-tropopause air into the lower midlatitude stratosphere. *Quarterly Journal of the Royal Meteorological Society*, *124*(549), 1559–1578.

Vogel, B., Günther, G., Müller, R., Grooß, J., Hoor, P., Krämer, M., & Riese, M. (2014). Fast transport from southeast Asia boundary layer sources to northern Europe: Rapid uplift in typhoons and eastward eddy shedding of the Asian monsoon anticyclone. *Atmospheric Chemistry and Physics*, *14*(23), 12–745.

Vogel, B., Müller, R., Günther, G., Spang, R., Hanumanthu, S., Li, D., & Stiller, G. P. (2019). Lagrangian simulations of the transport of young air masses to the top of the Asian monsoon anticyclone and into the tropical pipe. *Atmospheric Chemistry and Physics*, *19*(9), 6007–6034.

Wales, P. A., Salawitch, R. J., Nicely, J. M., Anderson, D. C., Canty, T. P., Baidar, S., et al. (2018). Stratospheric injection of brominated very short-lived substances: Aircraft observations in the Western Pacific and representation in global models. *Journal of Geophysical Research: Atmospheres*, *123*, 5690–5719. https://doi.org/10.1029/2017JD027978

Wang, X., Wu, Y., Tung, W.-w., Richter, J. H., Glanville, A. A., Tilmes, S., & Kinnison, D. E. (2018). The simulation of stratospheric water vapor over the Asian summer monsoon in CESM1 (WACCM) models. *Journal of Geophysical Research: Atmospheres*, *123*(20), 11377–11391. https://doi.org/10.1029/2018JD028971

Weinstock, E., Pittman, J., Sayres, D., Smith, J., Anderson, J., Wofsy, S., et al. (2007). Quantifying the impact of the North American monsoon and deep midlatitude convection on the subtropical lowermost stratosphere using in situ measurements. *Journal of Geophysical Research: Atmospheres*, *112*, D18310. https://doi.org/10.1029/2007JD008554

Wu, Y., Orbe, C., Tilmes, S., Abalos, M., & Wang, X. (2020). Fast transport pathways into the northern Hemisphere upper troposphere and lower stratosphere during northern summer. *Journal of Geophysical Research: Atmospheres*, *125*(3), e2019JD031552. https://doi.org/10.1029/2019JD031552

Wu, Y., & Shaw, T. A. (2016). The impact of the Asian summer monsoon circulation on the tropopause. *Journal of Climate*, *29*(24), 8689–8701.

Yan, X., Konopka, P., Ploeger, F., Podglajen, A., Wright, J. S., Müller, R., & Riese, M. (2019). The efficiency of transport into the stratosphere via the Asian and North American summer monsoon circulations. *Atmospheric Chemistry and Physics*, *19*(24), 15629–15649.

Yu, P., Toon, O. B., Neely, R. R., Martinsson, B. G., & Brenninkmeijer, C. A. (2015). Composition and physical properties of the Asian tropopause aerosol layer and the North American tropospheric aerosol layer. *Geophysical Research Letters*, *42*(7), 2540–2546. https://doi.org/10.1002/2015GL063181

Zhang, G. J., & McFarlane, N. A. (1995). Sensitivity of climate simulations to the parameterization of cumulus convection in the Canadian Climate Centre general circulation model. *Atmosphere-Ocean*, *33*(3), 407–446.